Self-compression of 1.8-μm pulses in gas-filled hollow-core fibers*

Rui-Rui Zhao(赵睿睿)[1,2], Ding Wang(王丁)[1], Yu Zhao(赵钰)[1,2], Yu-Xin Leng(冷雨欣)[1,†], and Ru-Xin Li(李儒新)[1]

[1] *State Key Laboratory of High Field Laser Physics, Shanghai Institute of Optics and Fine Mechanics, Chinese Academy of Sciences, Shanghai* 201800, *China*

[2] *University of Chinese Academy of Sciences, Beijing* 100049, *China*

(Received 8 April 2017; revised manuscript received 25 May 2017; published online 20 August 2017)

We numerically study the self-compression of the optical pulses centered at 1.8-μm in a hollow-core fiber (HCF) filled with argon. It is found that the pulse can be self-compressed to 2 optical cycles when the input pulse energy is 0.2-mJ and the gas pressure is 500-mbar (1 bar = 10^5 Pa). Inducing a proper positive chirp into the input pulse can lead to a shorter temporal duration after self-compression. These results will benefit the generation of energetic few-cycle mid-infrared pulses.

Keywords: spatiotemporal dynamics, self-compression, mid-infrared pulses, hollow-core fibers

PACS: 42.65.–k, 42.65.Re, 42.65.Jx, 42.81.Qb **DOI:** 10.1088/1674-1056/26/10/104206

1. Introduction

Ultrashort intense laser pulses are powerful tools for investigating ultrafast dynamics in high-field laser sciences such as high-order harmonic generation (HHG),[1] attosecond physics,[2,3] chemical-reaction dynamics,[4,5] and time-resolved measurements in atomic and molecular physics,[6] etc. Gas HHG is a significant process allowing the production of isolated attosecond pulses. This method involves focusing intense carrier-envelope phase-stabilized few-cycle driving laser pulses into a noble-gas target. The spectrum can be extended to the extreme ultraviolet (XUV) region. Because the HHG cutoff photon energy E_{co} and the laser central wavelength λ satisfy the relationship $E_{co} \sim I\lambda^2$,[7] the scaling laser–atom interaction towards a higher intensity with longer wavelengths is required, which can yield higher photon energies and shorter bursts of attosecond laser pulses.[8] Due to the balance between higher cut-off energy and moderate conversion efficiency of HHG, the infrared few-cycle laser pulses in a range of 1.5 μm–3 μm can be a suitable source for HHG.[9,10]

The hollow-core fiber (HCF) filled with noble gases has become an established pulse compressor for generating few-cycle intense femtosecond pulses. Compared with optical parametric chirped-pulse amplification and filamentation compression, the gas-filled HCF compressor offers a high-quality beam and beam-pointing stability because of its spatial-filtering characteristics.[11] In our previous work, Li *et al.*[12] experimentally demonstrated the generation of 0.7 mJ, 1.5-cycle laser pulses at 1.75-μm central wavelength, by spectral broadening of the pulse through a 1-m-long, 400-μm-diameter HCF filled with 400-mbar argon and the dispersion compensation. On the other hand, the temporal self-compression, which is a universal behavior of ultrashort pulses propagating in an anomalously dispersive nonlinear medium, is an alternative way to compress pulses.[13] Because of its advantage that no additional accurate dispersion compensation is needed, the self-compression process has become an attractive approach to producing few-cycle intense pulses. Gallmann *et al.*[14] obtained 0.35-mJ, 4.1-fs pulses with a central wavelength of 780-nm at a repetition rate of 3 kHz through a short 250-μm-diameter HCF filled with 2-bar neon. Kosareva *et al.*[15] achieved 0.38-mJ, 43-fs pulses and 0.84-mJ, 5.7-fs pulses in argon gas-filled HCFs with diameters of 100 μm and 200 μm, respectively, at a central wavelength of 800 nm and a repetition rate of 1 kHz. However, the self-compression in gas-filled HCFs to longer wavelengths has hardly been reported so far. Hauri *et al.*[16] used a 1-m-long HCF filled with 2-bar xenon to self-compress a self-phase stabilized 330-μJ, 55-fs pulse at 2 μm to below three optical cycles (17.9 fs) during the filamentary propagation. Mücke *et al.*[17] examined the self-compression of 2.2 mJ, 74.4 fs input pulses at 1.5 μm to 19.8 fs along a single filament in argon. Although these groups demonstrated self-compression with longer wavelength pulses, the results were all based on the filamentation. However, the filamentation is a highly dynamical process in both time and space domain, which depends on the delicate balance between self-focusing and plasma defocusing. The beam quality may not be as good as that from a waveguide. Thus, the investigation of spatiotemporal self-compression in the infrared region in gas-filled HCFs is desir-

*Project supported by the National Natural Science Foundation of China (Grant Nos. 61475169, 61521093, and 11127901), the Strategic Priority Research Program of the Chinese Academy of Sciences (Grant No. XDB16), and the International Science and Technology Cooperation Program of China (Grant No. 2016YFE0119300).

†Corresponding author. E-mail: lengyuxin@mail.siom.ac.cn

© 2017 Chinese Physical Society and IOP Publishing Ltd

able.

In this work, we numerically study the nonlinear propagation of intense 40-fs, 1.8-μm infrared pulses in a 250-μm-diameter and 1-m-long HCF filled with argon to explore self-compression. The pulse field is captured along both the laser propagating and transverse radical directions. By comparison with the cases of different gas pressures and initial pulse energies, the optimal conditions are determined to be 500 mbar and 0.2 mJ. The corresponding self-compressed pulse duration is ~ 14.7 fs. The influential factors affecting the spectral broadening are analyzed, which mainly depends on the Kerr effect in HCF. Moreover, to optimize the self-compression process, we induce some positive chirps into the input pulse. It is found that inducing a proper positive chirp can lead to shorter pulses after self-compression. The fused silica (FS) windows in the experiment can compensate for the pulse dispersion, thus the temporal duration of pulses chirped to 60 fs is eventually ~ 10.8 fs (less than 2 cycles). The remainder of this paper is organized as follows. Described in Section 2 is the theoretical model used in this work. In particular, the limit of gas-filled HCFs for self-compression is discussed. In Section 3 the self-compression simulation results are presented. By comparing pulses with different initial energies centered at 1.8-μm propagating in argon gas-filled HCFs at different gas pressures, the optimal self-compression conditions are determined. In Section 4 the experimental HCF FS window effect for self-compression of 1.8 μm output pulses is discussed. Finally, some conclusions are drawn from the present study in Section 5.

2. Theoretical model

The self-compression propagation dynamics of optical pulses in HCFs is simulated using the waveguide version of the unidirectional pulse propagation equation (UPPE), which is given as follows:[18]

$$\begin{aligned}&\partial_z U_m(\omega,z)\\ &= -\frac{\alpha_m}{2}U_m + \mathrm{i}\left(\beta_m - \frac{\omega}{v_\mathrm{g}}\right)U_m\\ &\quad + \frac{\omega}{c^2\beta_m(\omega)\cdot 2a^2\int_0^1 r\,\mathrm{d}r\,\mathrm{J}_0^2(u_m r)}\boldsymbol{e}_s\\ &\quad \times \int_0^a \mathrm{J}_0(u_m r/a)\left[\mathrm{i}\omega\frac{\boldsymbol{P}(r,\omega)}{\varepsilon_0} - \frac{\boldsymbol{j}(r,\omega)}{\varepsilon_0}\right] r\,\mathrm{d}r, \qquad (1)\end{aligned}$$

where U_m is the fiber-mode field, with the subscript m indicating the fiber-mode order; α_m and β_m are the linear attenuation and dispersion of the fiber mode, respectively;[19] v_g is the group velocity of the fundamental mode at the central wavelength of the pulse; $\mathrm{J}_0(u_m r/a)$ describes the mode field distribution and is a zero-order Bessel function of the first kind; u_m is the m-th zero point of $\mathrm{J}_0(x)$; ω, a, c, and ε_0 are the angular frequency, fiber inner radius, light speed, and permittivity in a vacuum, respectively; $P(r,\omega)$ and $j(r,\omega)$ describe the nonlinear polarization and plasma effects, respectively. The electric field of a pulse in the temporal domain can be reconstructed as follows:

$$E(x,y,z,t) = 2\cdot\mathrm{Re}\left\{\mathrm{FFT}^{-1}\left[\sum\nolimits_m U_m(\omega,z)\times\mathrm{J}_0(u_m r/a)\right]\right\}, \qquad (2)$$

where $\mathrm{Re}\{\cdots\}$ indicates the real part of a quantity, and $\mathbf{FFT}^{-1}$ is the inverse Fourier transform; $|E|^2$ is normalized according to the optical intensity. For the cubic Kerr effect, the nonlinear polarization is $P/\varepsilon_0 = 2n_0 n_2 \mathcal{I} E$, where $\mathcal{I}$ is the optical pulse-intensity envelope. The gas-ionization effect in the temporal domain is modeled by $j(t)/\varepsilon_0 = cn_0 W(\mathcal{I}) U_\mathrm{i}(\rho_\mathrm{nt}-\rho)E/\mathcal{I}$, where $W(\mathcal{I})$ is the ionization rate calculated according to the Perelomov–Popov–Terentiev (PPT) model;[20] U_i is the ionization potential; ρ is the electron density; ρ_nt is the neutral density of the gas. The plasma effect in the frequency domain is modeled by

$$\frac{j(\omega)}{\varepsilon_0} = \frac{\tau_\mathrm{c}(1+\mathrm{i}\omega\tau_\mathrm{c})}{1+\omega^2\tau_\mathrm{c}^2}\frac{e^2}{\varepsilon_0 m_\mathrm{e}}\mathrm{FFT}[\rho E],$$

where e, m_e, and τ_c are the electron charge, mass, and collision time, respectively. The ionization rate obtained using the PPT model is higher than that obtained using the Ammosov–Delone–Krainov (ADK) model;[21] thus, the simulation results based on the PPT rate differ from those based on the ADK rate. However, the qualitative behaviors are the same for both models. Assuming that the electrons are created at rest, the electron density ρ evolves as

$$\partial_t \rho = W(\mathcal{I})(\rho_\mathrm{nt}-\rho) + \sigma\mathcal{I}\rho/U_\mathrm{i}, \qquad (3)$$

where σ is the impact ionization cross section.

Equation (1) is integrated using the fourth-order Runge–Kutta method with self-adaptive step-length and error control. The input pulses are Gaussian and assumed to couple optimally into the fiber, i.e., with 98% pulse energy coupled to the fundamental mode. To ensure the convergence of the results, simulations of different numbers of pulse modes are conducted. These simulations yield the same results, indicating that the model is correct and can simulate the real propagation dynamics of self-compression in HCFs.

The design criteria for HCF compressors have been outlined.[22] First, the peak power of the pulse should not exceed the critical power level of self-focusing, which imposes an upper limit on the nonlinear refractive index and practically determines the gas type and the maximal pressure. Second, the peak intensity should not exceed the threshold at which photoionization becomes non-negligible (the nonlinear phase shift introduced by the free electrons emerging from ionization is comparable to that arising from the Kerr effect). This sets a lower limit for the HCF inner diameter. These criteria restrict the spectral-broadening capability of gas-filled HCF

compressors; thus, careful selection of the parameters of gas-filled HCFs is required.

Self-compression results from the interaction of waveguide dispersion and self-phase modulation (SPM). Pure SPM cannot change the pulse envelope but can only broaden the spectrum and induce an almost linear positive chirp. The waveguide structure can provide a negative dispersion that compensates for the positive dispersion introduced by the SPM effect, resulting in a small compression of the pulse. Therefore, the question whether it is possible to achieve a greater degree of self-compression under certain conditions arises. To the best of our knowledge, the waveguide dispersion depends on fiber diameter; for small diameters, the negative dispersion in HCFs is large. Thus, small-diameter HCFs should yield greater compression. On the other hand, diameters that are too small lead to large waveguide losses as follows:

$$\alpha_m = \left[\frac{U_m}{2\pi n_{\text{core}}(\omega)}\right]^2 \frac{\lambda^2}{a^3} \frac{n^2(\omega)+1}{\sqrt{n^2(\omega)-1}}, \tag{4}$$

where $n_{\text{core}}(\omega)$ and $n(\omega)$ are the refractive indices of the fiber core and fiber clad, respectively.

Moreover, as the mode area decreases, the nonlinear effect becomes more intense and can generate strong modulation into the pulse envelope in the temporal domain, destroying its linear chirp; i.e., it restricts the input pulse energy to a low range to prevent the pulse from breaking up. In practice, it is difficult to achieve sub-cycle intense infrared pulses in large-diameter HCFs. As a result, there should be a balance between the HCF inner diameter and the parameters of the incident pulse.

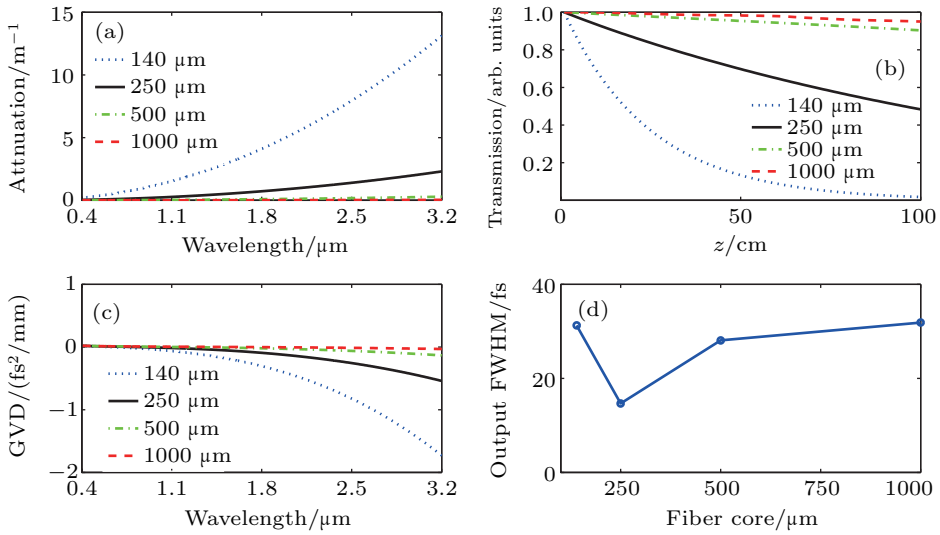


Fig. 1. (color online) (a) and (c) Power attenuation and GVD for different wavelengths ranging from 0.4 μm to 3.2 μm. (b) and (d) Transmission and FWHM of output pulses with respect to HCF diameter.

Considering these issues, we investigate the influence of a gas-filled HCF inner diameter on self-compression. Figures 1(a) and 1(c) show the plots of the power attenuation and group velocity dispersion (GVD) of the fundamental mode versus wavelength ranging from 0.4 μm to 3.2 μm, for four different typical HCF inner diameters. We choose the four kinds of HCFs because they are most commonly used in experiment. The hollow waveguide loss is largest in a 140-μm HCF, and there is a significantly increasing trend for longer wavelengths. Figure 1(b) shows the pulse transmittances. For a 140-μm HCF, it also exhibits a dramatic decline. As self-compression occurs due to the delicate balance between the SPM effect and anomalous dispersion, from Fig. 1(c), it is shown that HCFs with 140- and 250-μm inner diameters can provide decent anomalous dispersion while HCFs with 500- and 1000-μm diameters cannot support self-compression under the conditions considered above. In fact, the anomalous dispersion comes from the waveguide effect. The larger the diameter, the weaker the waveguide effect is. On the other hand, another important factor we should consider is the input pulse energy. If the input pulse energy is high enough, ionization and plasma effects also come into force and affect the self-compression. In order to achieve higher output energy, the HCF diameter should be large to avoid these effects. Therefore, 250 μm is the relatively optimal HCF diameter size for self-compression at 1.8-μm central wavelength with high pulse energies. In the current experimental conditions, generally the duration of 1.8-μm input pulses is 40 fs, and the corresponding energy is hundreds of μJ. Here we use 40 fs/1.8 μm pulses with 0.06-, 0.2-, 0.8-, and 3.2-mJ energies propagating through 500-mbar argon gas-filled HCFs with 140-, 250-, 500-, and 1000-μm diameters, respectively, keeping the light intensity the same, where no pulse breakup appears and self-compression can reach a desirable degree. According to the full widths at half maximum (FWHMs) of output pulses through HCFs with these four typical diameters,

we plot a linked curve to describe the changing tendency in Fig. 1(d). It can be seen that the FWHM of the output pulse in a 250-μm-diameter HCF is shorter than those in the other HCFs. When all the factors are taken into account, it is found that the 250-μm-diameter HCF can appropriately support the self-compression.

Because of its modest nonlinear index among noble gases, argon is widely used for the formation of the self-compression phenomenon.[23] To maintain high quality, the length of HCFs is limited to 1 m, owing to the technological limitations of HCFs arising from their rigidity.

3. Simulation results

Here, we employ a 250-μm-inner-diameter, 1-m-long argon gas-filled HCF, and use a 40-fs, 1.8-μm laser pulse for self-compression. In practice, this pulse can be normally obtained from a three-stage near-infrared optical parametric amplifier pumped by a commercial 4 mJ, 40-fs Ti:sapphire laser at 1-kHz repetition rate. The output energy is usually hundreds of μJ. The simulation initial parameters are also similar to those of the reported experimental conditions.[24] Under these parameters, we perform calculations for the cases of 0.3-, 0.4-, and 0.5-mJ pulses at 250 mbar; 0.1-, 0.2-, and 0.3-mJ pulses at 500 mbar; and 0.05-, 0.1-, and 0.15-mJ pulses at 1 bar. Pulses with various initial energies at a higher gas pressure are not explored, because for the 0.15-mJ low-energy pulse at 1 bar, the undesired supercontinuum over an octave appears. Further increasing the gas pressure would restrict input pulses with insufficient energy, on which the investigations and experiments are no longer worth being conducted.

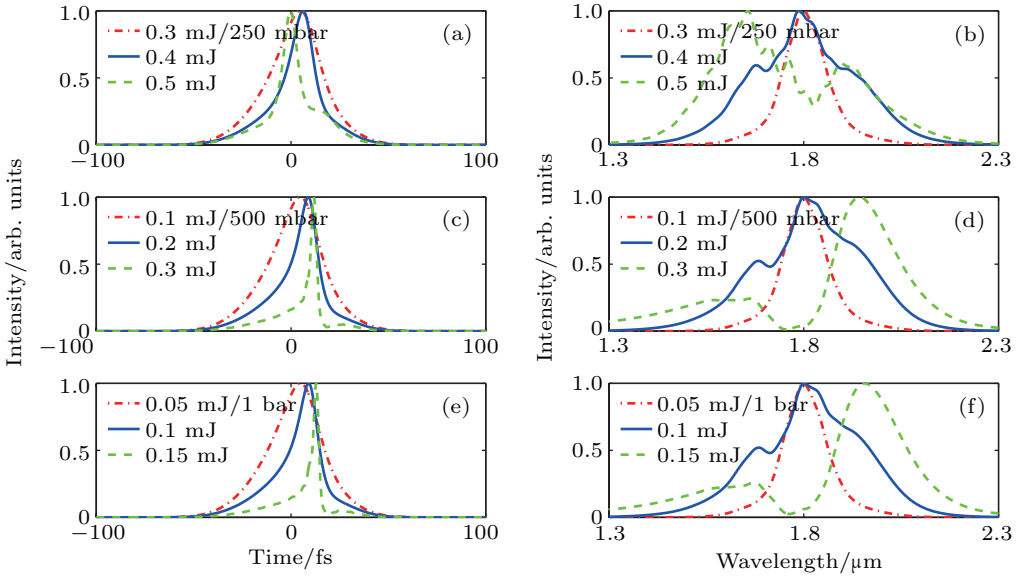


Fig. 2. (color online) Total output-pulse intensity profiles in panels (a), (c), (e) time and panels (b), (d), (f) frequency domains for pulses with different initial energies passing through 1-m-long argon gas-filled HCFs at different gas pressure: (a) and (b) 0.3-, 0.4-, and 0.5-mJ input pulses at 250 mbar; (c) and (d) 0.1-, 0.2-, and 0.3-mJ input pulses at 500 mbar; and (e), (f) 0.05-, 0.1-, and 0.15-mJ input pulses at 1 bar.

Figure 2 shows profiles of the total output-pulse intensity in time and frequency domains for the case where pulses with different initial energies propagate in HCFs at different gas pressures, obtained by integrating along the fiber-radius direction. Because the multimode coupled nonlinear UPPE is a function of fiber radius, where the pulse envelopes differ at different radii, the obtained pulse-envelope shape is made more concise by integrating along the fiber-radius direction. For input pulses of 0.4 mJ at 250 mbar, 0.2 mJ at 500 mbar, and 0.1 mJ at 1 bar, there is no pulse breakup, and the spectral broadening is maximized in an octave through self-compression. The corresponding pulse durations are 16.3, 14.7, and 15.4 fs, respectively. In contrast, using 500-mbar gas-filled HCFs to achieve 1.8-μm pulse self-compression is ideal. At the fiber outlet for a high or low gas pressure, the pulse is likely to split or fail to be compressed. Figure 3 shows the spatiotemporal intensity distributions of 0.1-, 0.2-, and 0.3-mJ pulses at 500 mbar. As shown by the fiber cross-section view, for 0.3 mJ, the pulse splits severely, and the bandwidth in the spatial domain exceeds one octave, indicating that the energy is too high. The spectral FWHM bandwidth for 0.2 mJ is wider than that for 0.1 mJ, both of which are within an octave. The temporal intensity envelope for 0.2 mJ is uniform and has a nearly ideal Gaussian shape. Thus, for pulses at a central wavelength of 1.8 μm in a 1-m-long, 500-mbar argon gas-filled HCF, setting the initial pulse energy to be 0.2 mJ is optimal. Moreover, because of the nonlinear refractive index of argon ($n_2 = 9.86 \times 10^{-20}$ cm^2/W), the corresponding critical power level of self-focusing is $P_{\rm cr} = \lambda^2/(2\pi n_0 \cdot n_2) \approx 26$ GW at 500 mbar. For 0.2-mJ/40-fs pulses passing through argon gas-filled HCFs, the input and output peak powers are approximately 5 GW and 6.8 GW, which are less than the $P_{\rm cr}$ at this time.

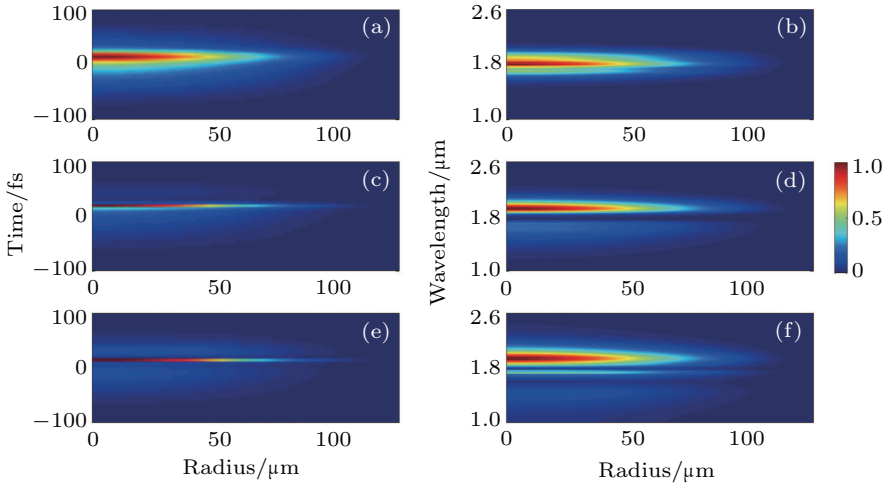


Fig. 3. (color online) Intensity distributions of the pulses in panels (a), (c), and (e) spatial time and panels (b), (d), and (f) spatial frequency domains for pulses with different initial energies passing through 1-m-long argon gas-filled HCFs at 500 mbar: (a), (b) 0.1 mJ, (c), (d) 0.2 mJ, and (e), (f) 0.3 mJ.

The propagation of intense few-cycle femtosecond pulses in gas-filled HCFs is a relatively complex nonlinear process. Accordingly, by studying the characteristics of the output pulses with the increase of the initial energies, we should be able to determine the main physical mechanism that influences the pulse self-compression propagation.

Figure 4 shows the spectra of output pulses with different initial pulse energies. With a low energy (0.1 mJ), the spectrum shape of the transmitted pulse is nearly identical to that of the incident pulse. As the energy of the input pulses increases, the output spectrum gradually becomes wider because the corresponding enhanced SPM effect generates new spectral components during the propagation in gas-filled HCFs. When the initial energy reaches 0.3 mJ, the bandwidth exceeds one octave, even reaches supercontinuum at a higher energy (0.5 mJ). Interestingly, a small blue preferred pedestal initially (0.2 mJ) appears in the spectral profile, which results from space–time focusing and self-steepening. Then for the 0.3-mJ case, not only is the blue pedestal broadened but also the center and peak of the pulse spectrum start to be red-shifted significantly, and almost no intensity is distributed at shorter wavelengths. The increase of the initial energy results in broadening on both the blue and red sides to a comparable extent. For higher energies of input pulses, additional red-shifting is likely to be induced by the competition between the Kerr and ionization effects,[25] corresponding to a sharp leading edge of the temporal pulse profile (marked with a green dash line in Fig. 2(c)). The question, which dominates the spectral broadening when the preferable spectrum is in an octave, arises. Next, we examine the pulse profiles at the fiber outlet by switching off each nonlinear effect separately. The Fourier-transform limit (FTL) pulse shape is also studied.

Figure 5 shows the total intensity profiles of output pulses for the cases with all effects and without plasma, without ionization, and without the Kerr effect, respectively. The FWHM of the self-compressed pulse is $\sim$ 14.7 fs, which is close to that of the FTL (11.6 fs), indicating that a significant degree of real-time dispersion compensation is introduced by the waveguide. The spectral shape without plasma or ionization is approximately the same as that with all the above effects, while the spectral line without the Kerr effect is significantly different from the others. This phenomenon illustrates that the Kerr effect is a main nonlinear factor influencing the pulse profile in the self-compression process when there are no filaments. It can produce self-focusing and induce SPM, broadening the spectrum. The temporal profile with all effects is asymmetric, owing to the sustained action of pulse steepening. Moreover, in Fig. 5(b), the resulting self-compressed pulse exhibits a flat spectral phase and is slightly positive chirped. The plasma can cause a negative refractive index, resulting in negative chirps on the pulse, whereas the SPM induces positive chirps, further demonstrating that the Kerr effect is the major factor affecting the pulse profile.

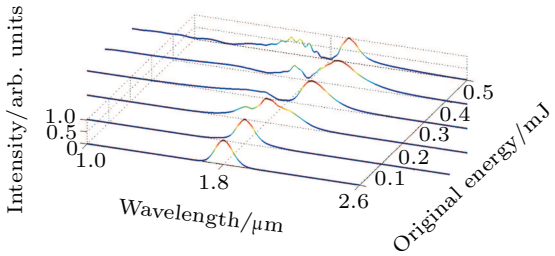


Fig. 4. (color online) Spectrum profiles of output pulses with different initial pulse energies.

In addition, to obtain more intense few-cycle infrared pulses, other methods could be used. The tapered HCF was used to adjust the dispersion and nonlinear effects by changing the HCF inner diameter via increasing the pulse propagation distance.[26] This method may improve self-compression to some extent; however, in an experiment, owing to complex technical constraints, it is difficult to acquire this kind of HCF.

Using the gas pressure-gradient is able to mitigate the ionization effect at the fiber inlet, but the beam spot may shake because of the gas liquidity. Inducing a chirp into the input pulse can reduce influences from ionization as well, which is easy to implement without disturbing light pulses, thus next we study its effect on self-compression.

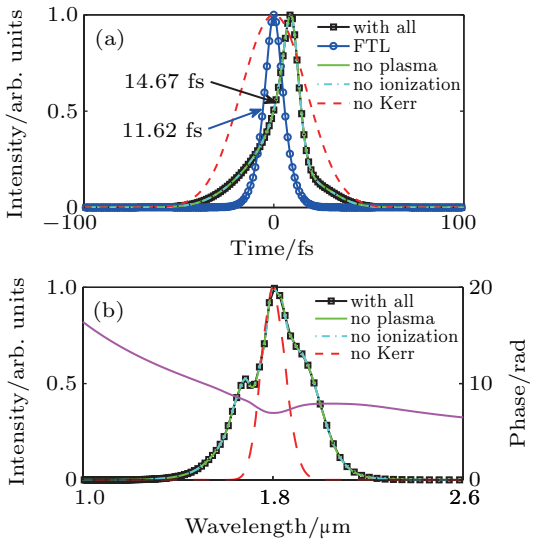


Fig. 5. (color online) (a) Time- and (b) wavelength-dependent intensity profiles of output pulses for the cases with all effects, without plasma, without ionization, and without the Kerr effect, respectively. The temporal profile of the FTL pulse is also shown.

Figure 6 shows the temporal intensity evolutions of pulses without chirps and with different positive chirps. Because the original 40-fs FWHM pulse is stretched by a chirp to 60 fs or 100 fs, its peak power becomes lower. This reduces the self-focusing effect, leading to higher transmittance. More importantly, inducing a positive chirp into the input pulse permits the initial energy to increase under the condition of no pulse breakup, which allows self-compression of pulses with high energy to be achieved and improves the beam quality. To compare self-compression at the same initial energy, here we choose to increase gas pressure for pulses with a positive chirp. It can be seen in Fig. 6(f) that the duration of pulse chirped to 100 fs at 3 bar is obviously much longer than that without being chirped. Due to limitations in experiments, the gas pressure should not be so high that further increasing gas pressure is not explored. Note that the temporal width of pulse chirped to 60 fs at 1.3-bar significantly becomes narrower during propagation, and the spatiotemporal intensity distribution keeps uniform at the fiber outlet. Figure 7 shows the intensity profiles in time and frequency domains of output pulses without chirps and with different positive chirps. As shown in Fig. 7(a), though the initial duration of pulse with a positive chirp is stretched, the FWHM of pulse chirped to 60 fs at 1.3 bar after self-compression in HCFs is 11.8 fs, shorter than that without chirp (14.7 fs), which is mainly due to the interaction between the induced positive chirp and the SPM effect in HCFs, thus enhancing the spectral broadening.

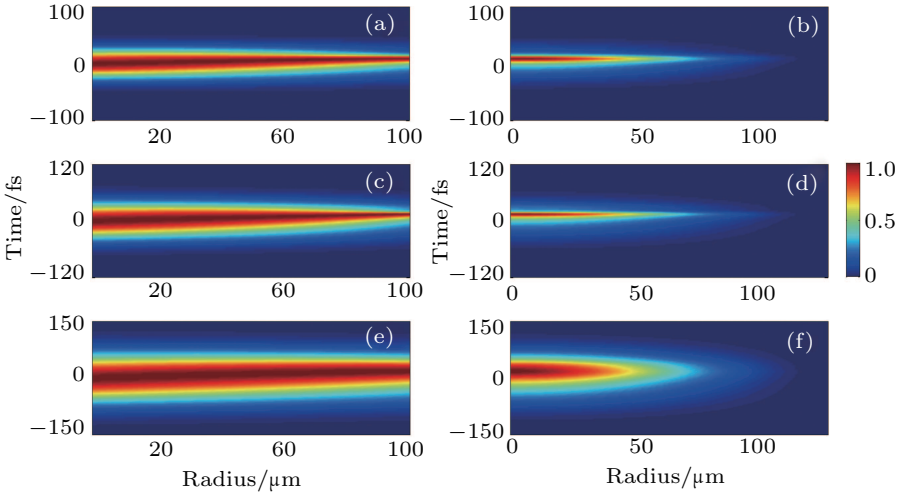


Fig. 6. (color online) Temporal intensity distributions along panels (a), (c), (e) propagating and panels (b), (d), (f) radical directions of pulses passing through 1-m-long argon gas-filled HCFs: (a), (b) without chirps at 500 mbar, (c), (d) with a positive chirp to 60 fs at 1.3 bar, and (e), (f) with a positive chirp to 100 fs at 3 bar.

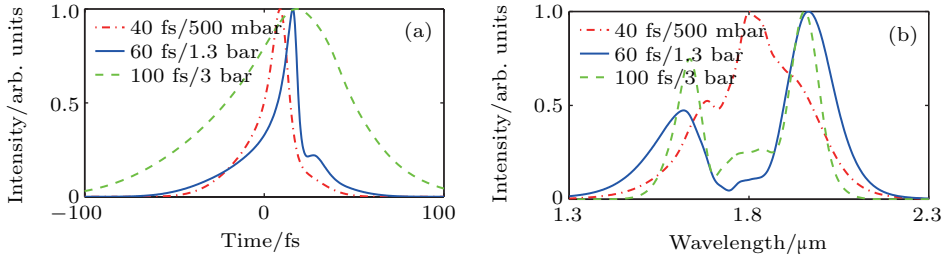


Fig. 7. (color online) (a) Time- and (b) frequency-dependent intensity profiles of output pulses in the cases without chirps at 500 mbar, with a positive chirp to 60 fs at 1.3 bar, and with a positive chirp to 100 fs at 3 bar.

In the real experiment, there are two pieces of 0.5-mm-thick FS windows forming into the Brewster angle at both the inlet and outlet of a gas-filled HCF, blocking the access of outside air. Due to the negative group delay dispersion (GDD) of the FS wedge in the spectral range of about 1.8 μm,[27] we calculate the duration of pulse with a positive chirp to 60 fs after self-compression and this FS compensation. Its FWHM can eventually reach to ∼ 10.8 fs (1.8 cycles).

4. Conclusions

We numerically study the self-compression propagation of 1.8-μm optical pulses in an HCF filled with argon. According to the UPPE model, the dynamic transmission and nonlinear self-compression of intense 1.8-μm pulses in an argon gas-filled HCF are simulated. Comparing the cases of different gas pressures and initial pulse energies, the optimal conditions are determined to be 500 mbar and 0.2 mJ. The corresponding pulse duration is ∼ 14.7 fs. The factors affecting the spectral broadening are analyzed, which mainly depend on the Kerr effect. After inducing different chirps into the input pulse, it is found that the pulses with a positive chirp to 60 fs can be self-compressed to shorter duration ∼ 11.8 fs at 1.3 bar. The influence of FS windows in the real experiment is also considered, which brings a negative GDD to the output pulses, thus the FWHM of pulse chirped to 60 fs is eventually ∼ 10.8 fs (less than 2 cycles). These results show that the method of inducing a proper positive chirp optimizes the self-compression process, which will benefit the generation of energetic few-cycle mid-infrared pulses.

References

[1] Zhou J, Peatross J, Murnane M M, Kapteyn H C and Christov I P 1996 *Phys. Rev. Lett.* **76** 752

[2] Scrinzi A, Ivanov M Yu, Kienberger R and Villeneuve D M 2006 *J. Phys. B* **39** 1

[3] Krausz F and Ivanov M 2009 *Rev. Mod. Phys.* **81** 163

[4] Zewail A H 1988 *Science* **242** 1645

[5] Suzuki T, Minemoto S, Kanai T and Sakai H 2004 *Phys. Rev. Lett.* **92** 133005

[6] Liu Y, Liu X, Deng Y, Wu C, Jiang H and Gong Q 2011 *Phys. Rev. Lett.* **106** 073004

[7] Corkum P B 1993 *Phys. Rev. Lett.* **71** 1994

[8] Sheehy B, Martin J D D, DiMauro L F, Agostini P, Schafer K J, Gaarde M B and Kulander K C 1999 *Phys. Rev. Lett.* **83** 5270

[9] Yakovlev V S, Ivanov M and Krausz F 2007 *Opt. Express* **15** 15351

[10] Vozzi C, Manzoni C, Calegari F, Benedetti E, Sansone G, Cerullo G, Nisoli M, Silvestri S De and Stagira S 2008 *J. Opt. Soc. Am. B* **25** B112

[11] Kaneshima K, Takeuchi K, Ishii N and Itatani J 2016 *High Power Laser Science and Engineering* **4** 17

[12] Li C, Wang D, Song L, Liu J, Liu P, Xu C, Leng Y, Li R and Xu Z 2011 *Opt. Express* **19** 6783

[13] Shen Y R 1984 *Principles of nonlinear optics* (New York: Wiley-Interscience) p. 575

[14] Gallmann L, Pfeifer T, Nagel P M, Abel M J, Neumark D M and Leone S R 2007 *Appl. Phys. B* **86** 561

[15] Kosareva O G, Panov N A, Uryupina D S, Kurilova M V, Mazhorova A V, Savel'ev A B, Volkov R V, Kandidov V P and Chin S L 2008 *Appl. Phys. B* **91** 35

[16] Hauri C P, Lopez-Martens R B, Blaga C I, *et al*. 2007 *Opt. Lett.* **32** 868

[17] Mücke O D, Ališauskas S, Verhoef A J, *et al*. 2009 *Opt. Lett.* **34** 2498

[18] Kolesik M and Moloney J V 2004 *Phys. Rev. E* **70** 036604

[19] Marcatili E A and Schmeltzer R A 1964 *Bell Syst. Tech. J.* **43** 1783

[20] Perelomov A M, Popov V S and Terent'ev M V 1966 *Sov. Phys.-JETP* **23** 924

[21] Ammosov M V, Delone N B and Krainov V P 1986 *Sov. Phys.-JETP* **64** 1191

[22] Vozzi C, Nisoli M, Sansone G, Stagira S and Silvestri De S 2005 *Appl. Phys. B* **80** 285

[23] Nagy T, Pervak V and Simon P 2011 *Opt. Lett.* **36** 4422

[24] Schmidt B E, Shiner A D, Lassonde P, Kieffer J C, Corkum P B, Villeneuve D M and Légaré F 2011 *Opt. Express* **19** 6858

[25] Champeaux S and Bergé L 2003 *Phys. Rev. E* **68** 066603

[26] Schenkel B, Biegert J, Keller U, Vozzi C, Nisoli M, Sansone G, Stagira S, Silvestri De S and Svelto O 2003 *Opt. Lett.* **28** 1987

[27] Schmidt B E, Béjot P, Giguère M, *et al*. 2010 *Appl. Phys. Lett.* **92** 121109